EFFECT OF POWDER LAYER COMPOSITION ON LASER SURFACE ALLOYING OF TITANIUM-NIOBIUM PARTS

JERONYMO, B.M.; RAMIREZ, A.F.; PLUA, A.I.; FOGAGNOLO, J.B.
FACULDADE DE ENGENHARIA MECÂNICA DA UNIVERSIDADE ESTADUAL DE CAMPINAS - FEM/UNICAMP
Rua Mendeleyev, 200 - CEP 13083-860
Cidade Universitária "Zeferino Vaz" Barão Geraldo
Campinas - SP
jeronymo92@gmail.com, Lattes, ID (Author)

ABSTRACT

Manufacturing metallic parts with compositional gradients through additive manufacturing makes it viable to obtain materials with property gradients, resulting in components with superior performance. The principles of the laser surface alloying technique can be applied to manufacture metallic materials with chemical gradients by using the technique of additive manufacturing by powder bed fusion. This work measures the response to the laser beam of layers of pre-mixed powders containing different proportions of titanium and niobium and dispersed on a commercially pure titanium substrate. As powders with different chemical compositions have different reflection rates to the laser beam, heat conduction and the volume of the weld pool vary depending on these characteristics. Isolated fusion beads were characterized by Scanning Electron Microscopy (SEM), Energy Dispersive X-Ray Spectroscopy (EDS), and Instrumented Indentation Testing (IIT). The results obtained should provide information on obtaining a dissimilar joint between commercially pure titanium and niobium.

***Keywords** (3 minimum – 5 maximum): Surface modification; Titanium substrate; Laser treatment; Niobium powder; Compositional gradient.*

INTRODUCTION

Functionally graded materials, which are considered advanced materials, are characterized by properties that vary along their dimensions (1). These gradients can be found in natural structures such as animal tissues, bones, teeth, and plants (2). In the biomedical field, components with elastic modulus gradients were initially proposed to address specific needs, such as to replicate the varying load-bearing behavior of different parts of bones (3) and to reduce the contact stress between the implant head and acetabular cup in hip replacements (4). Studies have shown that the elastic modulus of a material can influence osteoblast differentiation (5). Similarly, mechanical components made of titanium and its alloys can be designed with elastic modulus gradients. These gradients can be induced by controlling the microstructure through heat treatment (6) or by creating a chemical gradient through the controlled addition of alloying elements using techniques like LENS (Laser Engineered Net Shaping) (7).

Titanium and its alloys are highly valued in various industries, including aerospace, naval, chemical, and medical implant manufacturing, due to their high mechanical strength, low density, low elastic modulus, excellent biocompatibility, specific strength, low magnetic susceptibility and high corrosion resistance (8). These features help reduce the stiffness mismatch between the implant and the surrounding bone tissue, known as "stress shielding", which can lead to bone resorption and implant failure. However, these materials have high cost and limited corrosion and oxidation resistance at high temperatures, primarily due to their strong affinity for oxygen. The premature failure of orthopedic implants often starts on the surface and is the result of combined corrosion, fatigue, and wear phenomena (9). Generally, titanium and its alloys exhibit inadequate tribological properties, such as a high coefficient of friction and low hardness, limiting their use in applications involving severe wear and friction (10), such as joint replacements in the human body.

The elastic properties of titanium alloys can be modified through compositional changes or localized heat treatments. This ability to manipulate the material's behavior is of great interest in biomaterials research, given that it may reduce even further the stress shielding effect. Using specialized equipment designed for surface modification, beads of Ti-Nb alloys were created on the surface of commercially pure Titanium parts using laser technology. This study focused on the influence of specific processing parameters on the characteristics of the resulting surface, including microstructural characterization and the resulting changes in elasticity and hardness. The primary goal was to investigate the laser surface alloying process to create gradients in elastic modulus and hardness on the titanium surface. Niobium was chosen for its biocompatibility and its ability to stabilize the β phase, which has a lower elastic modulus (11).

Niobium is a refractory element, making fabrication and processing more challenging. Recent studies (12) have shown that binary Ti-(10-25 wt%) Nb alloys are promising candidates for biomedical applications due to their mechanical properties and biological performance, with increased mechanical strength and no cytotoxic effects observed under evaluated conditions.

Producing titanium and titanium alloy parts with chemical gradients offers a potential solution to reduce the stiffness of orthopedic implants and mitigate the stress shielding effect, which results from the significant stiffness mismatch between metallic implants and human bone. Additive manufacturing technologies, such as Selective Laser Melting (SLM) and Electron Beam Melting (EBM), enable the production of parts with controlled properties and complex geometries. SLM, for example, produces parts from metal powder by selectively melting the material with a laser beam according to a pre-defined CAD model. The process takes place inside a thermally controlled chamber filled with inert gas (13).

The way laser radiation is absorbed by powdered materials differs from that of solid materials. Although metals typically have high reflectivity, powdered materials can absorb laser energy more efficiently. This is due to a phenomenon known as multiple reflections (14), where a portion of the incident laser radiation first interacts with the outer surface of the powder particles. Here, some of the radiation is reflected, while the rest is absorbed. Simultaneously, another portion of the laser radiation penetrates deeper into the powder layer, where it undergoes further partial absorption and reflection. As these reflections continue, the laser radiation can penetrate beyond the average diameter of the powder particles, allowing deeper penetration into the powder layer. This ongoing interaction with particles within the pre-deposited powder layer ultimately leads to complete absorption of the laser energy (15).

This multiple reflection phenomenon enables the laser energy to reach the underlying substrate, facilitating its fusion. When both the powder and substrate melt, they create a fusion zone where the materials mix. The characteristics of this fusion zone depend on the amount of energy supplied to the system, leading to different fusion zone formations (16). In this research, three distinct types of fusion zone formations were observed: U-formation, conduction, and keyhole. Each formation observed during the study is described below.

The "U" shape formation in the laser-treated material is one variation of the fusion zone shape. This formation is caused by a phenomenon known as splashing (17), where Marangoni flows (18) drive the material to the edges of the fusion zone, resulting in a U-shaped cross-section. This shape is typically seen at lower laser powers, where the fused material in the powder layer tends to agglomerate and does not distribute evenly within the fusion zone (19).

The conductive fusion zone shape is desirable in additive manufacturing of dissimilar joints and other processes like laser surface modification. This formation results in a uniform fusion zone with a relatively smooth surface, offering benefits such as high process stability, reduced defects like pores and fractures, minimized vaporization of materials, and adequate penetration depth into the previous layer or substrate.

The keyhole shape is used in laser additive manufacturing and other processes where a high depth-to-width ratio in the weld bead is needed. In this case, the laser's high energy density is enough to vaporize the material and form an intense plasma. This process creates a cavity in the melt pool, resembling a keyhole. The plasma formed above the material's surface is called plume plasma, while the plasma inside the keyhole cavity is known as keyhole plasma (20). The main challenge of the keyhole formation is its inherent instability and the potential formation of porosity, which occurs when the vapor cavity collapses. The stability of the keyhole depends on the balance between surface tension pressure, which tends to close the keyhole, and vapor pressure, which keeps it open. The keyhole mode is characterized by deep penetration and high efficiency in laser radiation absorption (21).

MATERIALS AND METHODS

The titanium plates used in this study were obtained from Titânio Brasil LTDA, with a purity of 99.81%. Ti-42Nb Prealloyed Powder, with a composition of 42 wt% Nb, was used for alloying. Commercially Pure Titanium powder, also from Titânio Brasil LTDA, with a purity of 99.81%, was used to reduce the Niobium concentration for the first sample effectively by half. Commercially Pure Niobium powder, with a purity of 99.99%, was supplied by CBMM and used both pure and mixed in equal parts (in weight) with the prealloyed powder. Summarizing, to achieve compositions of 21 wt% Nb and 71 wt% Nb (samples 1 and 3), mixtures of pure titanium, Ti-42Nb and pure niobium powders were prepared in 50-50 weight ratios and deposited onto the substrate.

All experiments were conducted using equipment from *MBraun*, specifically within a glovebox chamber that allows for controlled atmospheric conditions. Since oxygen can significantly affect the outcomes of laser treatment on titanium (22), the atmosphere inside the chamber was maintained under positive argon pressure. The argon was purified through a filter bed to remove oxygen, ensuring an inert environment.

The laser employed in this study was a Ytterbium Fiber laser (IPG Photonics, model YLR) with a maximum power output of 500 W and a wavelength of 1.06 μm. The power settings for each sample were 30% (150 W), 60% (300 W) and 90% (450 W) of the maximum output.

Titanium plates with a thickness of 0.25 mm, previously prepared according to protocols from prior studies (13,16,23,24), were further sanded and cleaned using ethyl alcohol. Inside the glovebox, the plates were carefully covered with the prepared powder mixtures, with each plate handled separately to prevent cross-contamination. Single track laser samples were produced using various laser power settings, after which the samples were prepared for metallographic analysis. The plates were sectioned perpendicular to the laser path using a diamond disk.

The samples were characterized using optical microscopy, scanning electron microscopy (SEM), and Energy Dispersive X-ray Spectrometry (EDS). Mechanical properties such as hardness and elastic modulus were determined using a CSM model NHT1 instrumented indenter. The Berkovich diamond indenter was operated with a 300 mN load applied for 15 seconds at about 2250 nm depth, at a transient rate of 600 mN/min. Hardness and Young's modulus values were calculated using the Oliver and Pharr method, assuming a Poisson's ratio of 0.34. This analysis aimed to evaluate the mechanical behavior of the laser-modified regions. Multiple measurements were taken at different depths within the melt pool, ensuring consistent spacing from the surface.

The experimental setup included varying the laser power between 150 W and 450 W while keeping other parameters constant: CNC speed at 10 mm/s, laser spot diameter at 0.2 mm, and layer thickness at 0.25 mm. The resulting Ti-Nb compositions were analyzed for each laser power setting, as depicted in the accompanying image summarizing the single laser tracks.

RESULTS AND DISCUSSION

Table 1 displays the qualitative analysis from the EDS technique and the mean results from the mechanical tests on the samples. The crosses on Table 1 mark where an average was taken from the diluted phase. Some samples presented several phases, notably the ones produced with combined low energy and high concentrations of Nb. Unmelted Niobium powder, when evident, was not calculated into the atomic concentration averages or mechanical properties. The same logic was applied to the Titanium substrate; when measuring, it was determined that the end of indentations would occur when the value approached the expected for commercially pure Titanium for two consecutive measures.

Table 1. Percentage by weight of the chemical elements obtained by EDS, average Young's Modulus and Hardness Vickers for each sample, obtained by IIT.

Sample	Track Power (W)	Ti (%)	Nb (%)	E (GPa)	Hardness (HV)
1. $TiNb_{21\%}$	**150**	84.7	15.3	74 ± 17	262 ± 37
	300	97.0	3.0	107 ± 7	247 ± 19
	450	99.1	0.9	114 ± 6	233 ± 15
2. $TiNb_{42\%}$	**150**	54.7	45.3	85 ± 21	256 ± 31
	300	89.4	10.6	102 ± 17	250 ± 30
	450	92.3	7.7^{+}	100 ± 10	264 ± 15
3. $NbTi_{29\%}$	**150**	37.7	62.3^{+}	107 ± 34	220 ± 43
	300	82.8	17.2^{+}	99 ± 30	226 ± 18
	450	84.7	15.3^{+}	69 ± 2	239 ± 8
4. Nb_{cp}	**150**	39.9	60.1	109 ± 14	253 ± 20
	300	67.1	32.9	120 ± 22	258 ± 80
	450	68.8	31.2^{+}	98 ± 22	256 ± 21

Figure 1 shows the MEV images and the marks where the EDS analysis were taken from all samples. A visual comparison between varying concentrations of niobium on single laser tracks, with clear differences in their shape resulting from the laser treatment at different energy outputs is shown. The incomplete melting of the powder into the substrate is evident in the first row (150 W) as a result of the low power input on the tracks, which makes the fusion zone small, and little amount of Ti substrate is affected by it (conduction formation). In the second row, an intermediate power output (300 W) generates results between conductive and keyhole shape form pools, except for the U-formation at sample 3 ($NbTi_{29\%}$). Finally, the third row shows how the different powders reacted to 450 W of laser power, showing keyhole characteristic shape, with different behavior between columns due to crescent concentrations of Niobium with each image, as pointed in the schematics to the left and below the images.

Figure 1. MEV images of fusion beads produced organized by laser power and by Niobium (Nb) concentration (crescent, indicated by arrows), schematized.

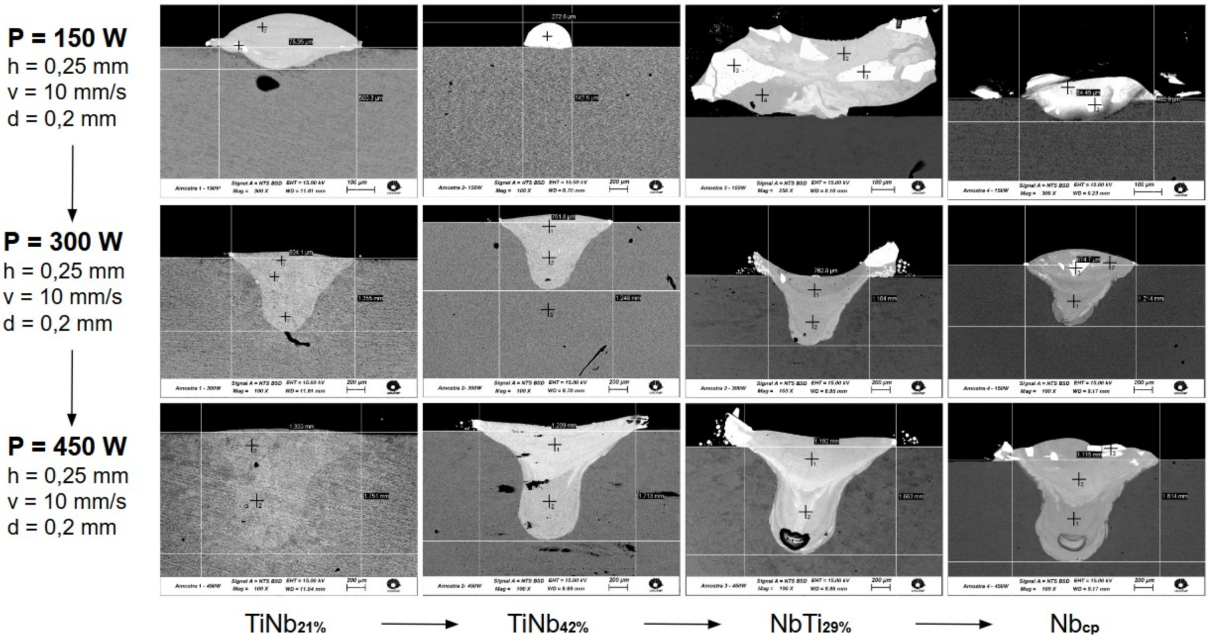

Despite the scale, some porosity and defects are already noticeable within the welding pools and at the underlying substrate in some samples, which are undesirable for achieving resistance to both impact and cyclic loads.

Most measures of Nb concentrations shown at Table 1 are lower in weight than the content in the powder layer before the laser treatment. This can be explained both by the unmelted phase (segregation) and the addition of Titanium from the substrate, where the energy was enough to melt both Ti powder and substrate. In the cases of $NbTi_{29\%}$ and Ni_{cp} at 450 W, pores are generated at the bottom of the fusion zone, caused by the evaporation of small amounts of substrate. In addition, small Nb unmelted particles are observed at the top of the fusion zone. Figure 2 (a-b) shows in more detail the splashing of unmelted Nb pores on the surface. Figure 2-a also shows the formation of a cavity at the pool base, observed frequently when the keyhole shape occurs (20).

Figure 2. MEV image and EDS analysis of $NbTi_{29\%}$ single laser track at 450 W (a). Surface view of the untreated sample, using optic microscope (b).

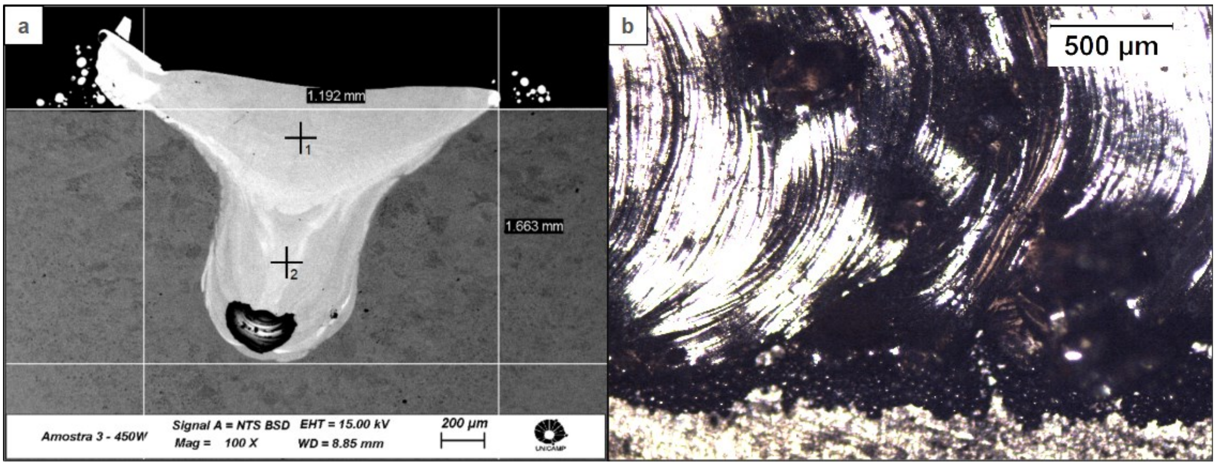

Table 2 shows the MEV imaging measurements for the characteristic welding pool dimensions for each track and sample. The measurements for the 150 W track that did not truly weld powder and substrate were not made.

Table 2. Weld pool measures for samples 1-4 at each power output.

Sample	Track Power (W)	full width (µm)	in-substrate depth (µm)	outer height (µm)	depth-to-width (ratio)
1. $TiNb_{21\%}$	**150**	500.3	79.0	120.3	0.16
	300	1355.0	804.1	71.6	0.59
	450	1751.0	1333.0	55.1	0.76
2. $TiNb_{42\%}$	**150**	542.5	-	272.6	0
	300	1248.0	751.8	88.1	0.60
	450	1713.0	1209.0	184.5	0.71
3. $NbTi_{29\%}$	**150**	-	-	-	0
	300	1104.0	762.8	391.1	0.69
	450	1663.0	1192.0	181.8	0.72
4. Nb_{cp}	**150**	492.9	84.5	83.5	0.17
	300	1214.0	674.7	184.5	0.56
	450	1614.0	1115.0	234.1	0.69

The analysis considers different refractivity and reflectivity of niobium in comparison to titanium as one of the reasons for the differences in measures shown in the tables. Another phenomenon observed is the varying dilution from substrate in the welding process with the same power output, by changing the powder composition. This can be explained by the differences in atomic mass, melting points and optic properties that affect the multiple reflection phenomenon.

Figure 3. IIT measuring results for sample 4-Nb$_{cp}$. Calculated measures for Young's Modulus (a) and Hardness Vickers (b).

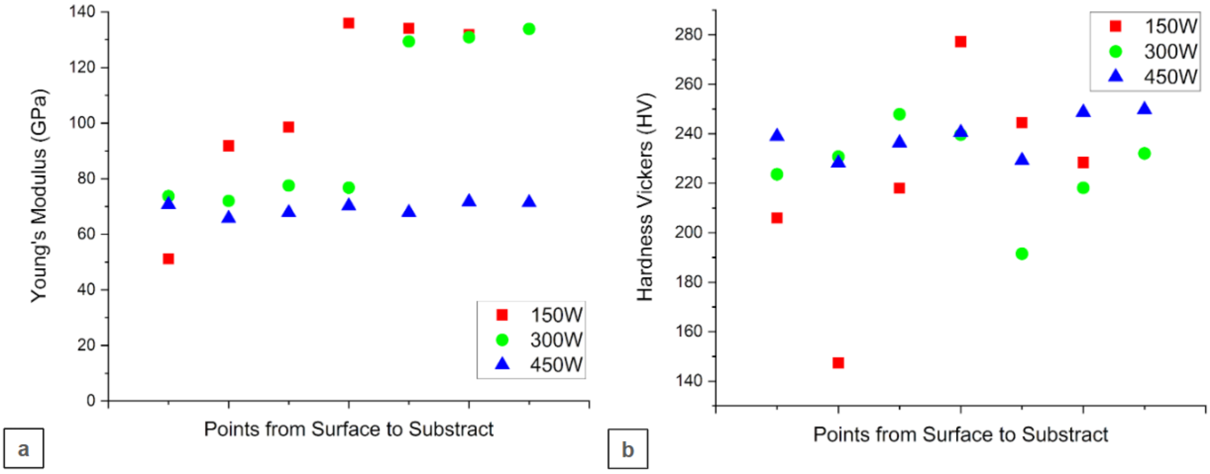

The mechanical testing on the samples (example shown in Figure 3) show a complex behavior between the concentration of Niobium and the results. The microstructure achieved (i.e the atomic arrangement) with each process is the probable cause and further investigation is needed (by using techniques unavailable to single tracks, such as X-Ray Diffraction Spectroscopy). In general, better results for the objective set for this study (low E and high HV values) were obtained either with low power and Nb concentration (at the cost of low penetration) or with high energy and concentration (at the cost of high porosity or keyhole cavity). High concentrations of Niobium frequently result in phase separations and incomplete melting of powders, which may be mitigated by making full coatings with appropriate strategies for laser paths, instead of single tracks (object of this study). Figure 3 also shows the trend for great variability of measures according to the region of the indentation, especially for tracks where low energy was applied. High concentration and thermal gradients result in great property gradients measured as well. Where high laser power was applied, the measures for both Young's Modulus (stiffness) and Hardness Vickers (which indicates tensile strength) have lower deviations.

CONCLUSION

The process of single tracks production and measurement were carried out successfully, showing meaningful differences between each set of parameters. The biomaterial in contact with bone tissue should have an elastic modulus close to the measured for bone tissue (<40GPa) to avoid stress shielding and high hardness to guarantee its life cycle when facing stress solicitations. The coatings that come closest to the desired mechanical qualities were $NbTi_{29\%}$ and Nb_{cp} at 450 W laser power. They showed low elastic modulus and high hardness values. However, since the production of a functional part involves full coating, a lower setting for energy will probably have the best results (i.e. 300 W in an appropriate path strategy) when applied, since they minimize splashing, segregation and keyhole cavity formation, but also the heat affected zones overlap with each passing, resulting in lower gradients in properties when compared to the ones obtained with single tracks.

An interesting strategy for coatings may be using intermediate amounts of Niobium concentration and laser power to avoid property gradients too high and undesired porosity, which may lead to crack propagation and low life cycles.

The study highlights the importance of carefully controlling processing parameters to produce functionally graded materials that meet the stringent requirements for biomedical implants, particularly in reducing stress shielding effects and enhancing the durability of the implants under mechanical stress. Further investigations into full coatings and optimized laser path strategies are recommended to refine these findings and extend their applicability to practical manufacturing processes.

ACKNOWLEDGEMENTS

The authors would like to thank the Brazilian Federal Agency for Support and Improvement of Higher Education (CAPES, Brazil) for the scholarship granted to the first 3 authors.

REFERENCES

1. MAHAMOOD, R.M.; AKINLABI, E.T.; SHUKLA, M.; PITYANA, S. Functionally graded materials: An overview. Proceeding of the world congress on engineering (WCE 2012), v.3, July 4-6, London, U.K., 2012.

2. KNOPPERS, R.; GUNNINK, J.W.; VAN DEN HOUT, J.; VAN VLIET, W. The reality of functionally graded material products, in: Pham, D.T.; Eldukhri, E.E.; Soroka, A.J. (Eds.), Intelligent Production Machines and Systems, Elsevier, Great Bretain, 2005, p.38-43.

3. GANESH, V.K.; RAMAKRISHNA, K.; GHISTA, D.N. Biomechanics of bone-fracture fixation by stiffness-graded plates in comparison with stainless-steel plates. Biomed. Eng. Online, v.4, n.46, p.31, 2005. DOI: 10.1186/1475-925X-4-46.

4. FOUAD, H. In vitro evaluation of stiffness graded artificial hip joint femur head in terms of joint stresses distributions and dimensions: finite element study. J. Mater. Sci. Mater. Med., v.22, n.6, p.1589-1598, 2011.

5. CHATTERJEE, K.; LIN-GIBSON, S.; WALLACE, W.E.; PAREKH, S.H.; LEE, Y.J.; CICERONE, M.T.; YOUNG, M.F.; SIMON JR, C.G. The effect of 3D hydrogel scaffold modulus on osteoblast differentiation and mineralization revealed by combinatorial screening. Biomater., v.31, n.19, p.5051-5062, 2010.

6. LOPES, E.S.N.; CONTIERI, R.J.; BUTTON, S.T.; CARAM, R. Femoral hip stem prosthesis made of graded elastic modulus metastable β Ti alloy. Mater. Design, v.69, p.30-36, 2015.

7. HOFMANN, D.C.; ROBERTS, S.; OTIS, R.; KOLODZIEJSKA, J.; DILLON, R.P.; SUH, J.O.; SHAPIRO, A.A., LIU, Z.K.; BORGONIA, J.P. Developing Gradient Metal Alloys through Radial Deposition Additive Manufacturing. Sci. Rep., v.4, n.5357, 2014. DOI: 10.1038/srep05357.

8. GEETHA, M.; SINGH, A.K.; ASOKAMANI, R.; GOGIA, A.K. Ti based biomaterials, the ultimate choice for orthopaedic implants-A review. Prog. Mater. Sci., v.54, n.3, p.397–425, 2009.

9. TEOH, S.H. Fatigue of biomaterials: a review. Int. J. Fatigue, v.22, p.825–837, 2000.

10. TIAN, Y.S.; CHEN, C.Z.; WANG, D.Y.; LEI, T.Q. Laser surface modification of titanium alloys-a review. Surf. Rev. Lett., v.12, n.1, p.123-130, 2005.

11. SONG, Y.; XU, D.S.; YANG, R.; LI, D.; WU, W.T.; GUO, Z.X. Theoretical study of the effects of alloying elements on the strength and modulus of β-type bio-titanium alloys. Mater. Sci. Eng. A, v.260, p.269-274, 1999.

12. ZHANG Y, SUN D, CHENG J, TSOI JKH, CHEN J. Mechanical and biological properties of Ti-(0-25 wt%)Nb alloys for biomedical implants application. Regen Biomater. 2020;7(1):119-27. http://dx.doi.org/10.1093/rb/rbz042 PMid:32153995.

13. SALLICA-LEVA, E.; CARAM, R.; JARDINI, A.L.; FOGAGNOLO, J.B. Ductility improvement due to martensite α' decomposition in porous Ti-6Al-4V parts produced by selective laser melting for orthopedic implants. J. Mech. Behav. Biomed. Mater., v.54, p.149- 158, 2016.
14. KHAN, M.; DICKENS, P. Selective laser melting (SLM) of gold (Au). Rapid Prototyping J., v.18, n.1, p.81-94, 2012.
15. GUSAROV, A. Radiative transfer, absorption, and reflection by metal powder beds in laser powder-bed processing. Journal of Quantitative Spectroscopy and Radiative Transfer, Elsevier, v. 257, p. 107366, 2020.
16. FOGAGNOLO, J. B.; RODRIGUES, A.; LIMA, M. S. F. d.; AMIGÓ, V.; CARAM, R. A novel proposal to manipulate the properties of titanium parts by laser surface alloying. Scripta Materialia, Elsevier, v. 68, n. 7, p. 471–474, 2013.
17. ZAGADE, P.; GAUTHAM, B.; DE, A.; DEBROY, T. Analytical estimation of fusion zone dimensions and cooling rates in part scale laser powder bed fusion. Additive Manufacturing, Elsevier, v. 46, p. 102222, 2021.
18. KHAIRALLAH, S. A.; ANDERSON, A. T.; RUBENCHIK, A.; KING, W. E. Laser powder-bed fusion additive manufacturing: Physics of complex melt flow and formation mechanisms of pores, spatter, and denudation zones. Acta Materialia, Elsevier, v. 108, p. 36–45, 2016.
19. XU, P.-q.; LI, L.; ZHANG, C. S. Microstructure characterization of laser welded ti-6al-4v fusion zones. Materials characterization, Elsevier, v. 87, p. 179–185, 2014.
20. KIM, J.; WATANABE, T.; YOSHIDA, Y. Effect of the beam-defocusing characteristics on porosity formation in laser welding. Journal of materials science letters, Springer, v. 14, p. 1624–1626, 1995.
21. PANWISAWAS, C.; PERUMAL, B.; WARD, R. M.; TURNER, N.; TURNER, R. P.; BROOKS, J. W.; BASOALTO, H. C. Keyhole formation and thermal fluid flow-induced porosity during laser fusion welding in titanium alloys: Experimental and modelling. Acta materialia, Elsevier, v. 126, p. 251–263, 2017.
22. LI, X.; XIE, J.; ZHOU, Y. Effects of oxygen contamination in the argon shielding gas in laser welding of commercially pure titanium thin sheet. Journal of materials science, Springer, v. 40, p. 3437–3443, 2005.
23. CARVALHO, L. R. A. de; SALLICA-LEVA, E.; ENCINAS, E. R.; FOGAGNOLO, J. B. Less-rigid coating in ti obtained by laser surface alloying with nb. Surface and Coatings Technology, Elsevier, v. 346, p. 19–28, 2018.

24. FOGAGNOLO, J. B.; RODRIGUES, A. V.; SALLICA-LEVA, E.; LIMA, M. S.; CARAM, R. Surface stiffness gradient in ti parts obtained by laser surface alloying with cu and nb. Surface and Coatings Technology, Elsevier, v. 297, p. 34–42, 2016.